

Manuscript Number:	JTICE-D-21-01578
Article Type:	Original Paper
Section/Category:	Energy and Environmental Science and Technology
Keywords:	g-C ₃ N ₄ ; benzene, K ⁺ -co-doping; in situ H ₂ O ₂ production; Fenton-like; dye degradation
Abstract:	<p>Background: Fe²⁺/H₂O₂-based photo-Fenton process is often used in pollutions removal. But, iron residue related low activities at neutral condition hinder its practical applications. Activation of in situ-generated H₂O₂ for Fenton-like degradation of pollution through catalysts absences of Fe species is expected.</p> <p>Methods: A strip-like benzene and K⁺ co-doped g-C₃N₄ (KBCN) was constructed by the thermal polymerization of assemblies of melamine and 2-aminoterephthalic acid, then post-calcination in LiCl-KCl molten salt, which was then used to degrade Rhodamine B (RhB) and Congo red (CR) via in situ-generated H₂O₂.</p> <p>Significant findings : Benzene and K⁺ co-doping are critical both in increasing charge separation and enhancing the H₂O₂ production. The yield of H₂O₂ for KBCN is 57.5 μM in pure water after 60 min irradiation. In the absence of Fe²⁺, the in situ-generated H₂O₂ could subsequently to degrade RhB and CR with the formed ·OH. The apparent rate constants of KBCN for RhB and CR degradation were 0.0446 and 0.0497 min⁻¹, respectively. The advantages of degradation with in situ-generated H₂O₂ in the absence of Fe²⁺ can provide a new prospective to the environmental friendly Fenton-like reaction.</p>

Submission checklist

1. Is the manuscript double-spaced with a font size of 12 pt (Times or Times New Roman preferred)?

Yes

2. Have you given full addresses and affiliations for all co-authors?

Yes

3. Is the corresponding author identified by an asterisk (*) and their contact details (phone number and e-mail address) given on the first page?

Yes

4. Have you given a Graphical Abstract and Highlights of your manuscript?

Yes

5. Does the manuscript include a one-paragraph abstract of no more than 200 words for Original Papers or 150 words for Short Communications?

Yes

6. Do the length of manuscript and the number of display items obey the requirement? Have keywords (maximum 6) been provided immediately after the abstract?

Yes

7. Are sections given Arabic numbers with subsections numbered using the decimal system? NOTE: Acknowledgements and References sections are not numbered.

Yes

8. Do you embed all figures, tables, and schemes (including the captions) at appropriate places in the text?

Yes

9. Are References in the correct format for this journal?

Yes

10. Are all references mentioned in the Reference list cited in the text, and vice versa?

Yes

11. Has the manuscript been spell-checked and grammar-checked?

Yes

12. Are all symbols translated correctly in the pdf file?

Yes

13. Has written permission been obtained and uploaded as Additional Files for use of copyrighted materials from other sources (including illustrations, tables, text quotations, Web content, etc.)? Has the copyright information been included in the relevant figure caption or table footnote, as an example "Reprinted with permission from Ref. [10]. Copyright 2010 Elsevier"?

Yes.

- A precursor-engineering, molten-salt calcination method was used to modify g-C₃N₄.
- Benzene and K⁺ co-doped g-C₃N₄ can degrade RhB and CR with in situ-generated H₂O₂.
- Modified g-C₃N₄ exhibits enhanced charge separation, H₂O₂ and ·OH generation.
- 57.7 μM H₂O₂ was produced in water after 60 min, 22 times of that pure g-C₃N₄.
- 93.3% RhB and 96.6% CR were degraded after 60 min by H₂O₂-derived ·OH radicals.

1 **Enhanced Fenton-like degradation of Rhodamine B and Congo red by benzene**
2
3 **and K⁺ co-doped carbon nitride with in situ-generated H₂O₂**
4
5
6
7

8
9 Yanfang Chen^a, Xuemei Yan^a, Haifeng Lin^{a, *}, Chao Wang^a, Jixiang Xu^{a,*}
10
11
12

13
14 ^a*Key Laboratory of Eco-Chemical Engineering, Ministry of Education, State*
15 *Laboratory of Inorganic Synthesis and Applied Chemistry, College of Chemistry and*
16 *Molecular Engineering, Qingdao University of Science and Technology, Qingdao*
17
18
19
20 *266042, China*
21
22
23
24
25
26
27
28
29
30
31
32
33
34
35
36
37
38
39
40
41
42
43
44
45
46
47
48
49
50
51
52
53
54

55
56
57 * Corresponding authors: hflin20088@126.com (H.F. Lin); xujix47@163.com (X.J. Xu); +86
58

59 532-840-22681
60
61
62
63
64
65

Abstract

Background: $\text{Fe}^{2+}/\text{H}_2\text{O}_2$ -based photo-Fenton process is often used in pollutions removal. But, iron residue related low activities at neutral condition hinder its practical applications. Activation of in situ-generated H_2O_2 for Fenton-like degradation of pollution through catalysts absences of Fe species is expected.

Methods: A strip-like benzene and K^+ co-doped g- C_3N_4 (KBCN) was constructed by the thermal polymerization of assemblies of melamine and 2-aminoterephthalic acid, then post-calcination in LiCl-KCl molten salt, which was then used to degrade Rhodamine B (RhB) and Congo red (CR) via in situ-generated H_2O_2 .

Significant findings: Benzene and K^+ co-doping are critical both in increasing charge separation and enhancing the H_2O_2 production. The yield of H_2O_2 for KBCN is 57.5 μM in pure water after 60 min irradiation. In the absence of Fe^{2+} , the in situ-generated H_2O_2 could subsequently to degrade RhB and CR with the formed $\cdot\text{OH}$. The apparent rate constants of KBCN for RhB and CR degradation were 0.0446 and 0.0497 min^{-1} , respectively. The advantages of degradation with in situ-generated H_2O_2 in the absence of Fe^{2+} can provide a new prospective to the environmental friendly Fenton-like reaction.

Keywords: g- C_3N_4 ; benzene, K^+ -co-doping; in situ H_2O_2 production, Fenton-like; dye degradation

1. Introduction

In recent years, $\text{Fe}^{2+}/\text{H}_2\text{O}_2$ -based photo-Fenton process is widely used in pollutions removal via generated active hydroxyl ($\cdot\text{OH}$) radicals [1–4]. In such process, a lower solution pH for facilitating regenerative cycle of Fe^{3+} to Fe^{2+} and additional H_2O_2 are need, which is an uneconomical process. To avoid the introduction of H_2O_2 , photo-Fenton systems containing photocatalysts which can in situ generate H_2O_2 for degradation of pollutions are emerged. For example, Zhang et al. fabricated $\text{CdS}/\text{rGO}/\text{Fe}^{2+}$ system for in situ generation of H_2O_2 to degrade phenol at natural pH [5]. Liu et al. demonstrated a $\text{WO}_3/\text{g-C}_3\text{N}_4$, which displayed a highly enhanced activity for efficient oxidation of ciprofloxacin with in situ-generated H_2O_2 [6]. In those systems, a Fe-based species were needed to activate formed H_2O_2 for generation of $\cdot\text{OH}$ radicals. However, iron residue related second pollution and low activities at neutral condition hinder its practical applications [7]. Thus, activation of in situ-generated H_2O_2 for Fenton-like degradation of pollution through catalysts absences of Fe species is expected.

Generally, production of H_2O_2 can be achieved by anthraquinonoid autoxidation [8], electrochemical or photocatalytic synthesis [9]. Particularly, photocatalytic production of H_2O_2 from water and O_2 over semiconductors is a convenient way for *in situ* and on-demand production [10–13]. Moreover, the generated H_2O_2 can be decomposed with photogenerated electrons to produce $\cdot\text{OH}$ ($2\text{H}_2\text{O}_2 + \text{H}^+ + \text{e}^- = \text{H}_2\text{O} + \cdot\text{OH}$), which then can be applied to decompose organic compounds including dyes. Li et al. prepared black phosphorus/oxygen-enriched porous carbon nitride ($\text{g-C}_3\text{N}_4$, CN) for

1 H₂O₂ production and subsequent methyl orange degradation through produced ·OH
2
3 radical [14]. Sun et al. prepared black phosphorus/oxygen-enriched porous carbon
4
5 nitride (g-C₃N₄, CN) for Cu_xP/CN catalyst for the removal of various organic
6
7 contaminants by Fenton-like catalytic process [15]. Zhao et al. found that H₂O₂
8
9 production and decomposition were accelerated by KOH modified CN with high
10
11 electron-holes separation efficiency [16]. In this regard, design of a photocatalyst with
12
13 high charge separation to effectively produce H₂O₂ and then ·OH for pollutants
14
15 removal is encouraged.
16
17
18
19
20
21

22 At present, a series of semiconductor materials have been used for photocatalytic
23
24 H₂O₂ production [17–21]. Notably, CN has attracted many attentions due to its easy to
25
26 synthesis and a high selectivity for the oxygen reduction reaction [21–26]. However,
27
28 the photocatalytic H₂O₂ production performance of pristine CN (PCN) is not
29
30 satisfactory owing to its poor visible light response and rapid electron–hole
31
32 recombination. The poor electrons–holes separation is due to the symmetrical
33
34 tri-s-triazine ring of CN. Thus, methods like heteroatom doping, creation of
35
36 carbon/nitrogen vacancies, and integration of aromatic structures into the skeleton of
37
38 CN have been employed to break the symmetry of the tri-s-triazine ring and improve
39
40 the charge carriers separation [27–30]. Owing to similar aromatic structures and sizes,
41
42 the benzene has been incorporated into the CN backbone to regulate electronic
43
44 structure and catalytic performance of CN [31–35].
45
46
47
48
49
50
51
52
53
54

55 On the other hand, CN synthesized by conventional thermal polymerization of
56
57 nitrogen-containing precursors usually has abundant hydrogen bonds in the intralayer
58
59
60
61
62
63
64
65

1 framework [36], leading to a localization of photoexcited charge carriers within each
2
3 tri-s-triazine unit and poor intralayer charge transport [37]. Destroying these hydrogen
4
5 bonds is necessary to accelerate the charge transfer. It has been confirmed that thermal
6
7 treatment of CN with molten salt can tailor the grain boundary chemistry and
8
9 facilitate electron delocalization. Wang et al. used LiCl–KCl molten salt as the solvent
10
11 to tune the polymerization process of CN and obtained crystalline CN with high
12
13 charge separation efficiency [38–40]. In addition, Long et al. found that intercalated
14
15 K^+ acted as Lewis acid sites to facilitate alcohol oxidation and proton release [25],
16
17 leading to increased photocatalytic H_2O_2 production. Inspired by these facts, we
18
19 envisioned that simultaneous doping of benzene and K^+ into CN would be a viable
20
21 approach to achieve improved in situ H_2O_2 and $\cdot OH$ generation, then high pollutants
22
23 degradation via Fenton-like reaction. However, this has not been reported to the best
24
25 of our knowledge.
26
27
28
29
30
31
32
33
34
35

36 Herein, a benzene and K^+ co-doped CN (KBCN) was prepared by the thermal
37
38 polymerization of an assembly of melamine (MA) and 2-aminoterephthalic acid
39
40 (MA–ATA), followed by post-calcination in LiCl–KCl mixture, which was then used
41
42 as a Fenton-like catalysts to degrade Rhodamine B (RhB) and Congo red (CR). The
43
44 strip-like KBCN exhibited excellent H_2O_2 yield with value of 57.7 μM in pure water
45
46 after 60 min irradiation, and high Fenton-like degradation performance for RhB and
47
48 CR with apparent rate constants of 0.0446 and 0.0497 min^{-1} , respectively. The
49
50 mechanisms of enhanced H_2O_2 production, RhB and CR degradation were discussed.
51
52
53
54
55
56
57
58
59 Our results presented here open a novel route for efficient wastewater treatment.
60
61
62
63
64
65

2. Experimental Section

2.1. Raw materials

All used reagents were analytically pure and directly used without purification. Melamine, Rhodamine B (RhB), Congo red (CR), lithium chloride (LiCl), and potassium chloride (KCl), and benzoquinone (BQ) were obtained from Sinopharm Chemical Reagent Co., Ltd. (Shanghai, China). 2-aminoterephthalic acid (ATA) and terephthalic acid (TA) were purchased from Aladdin Bio-Chem Technology Co., Ltd. Ethanol and tert butyl alcohol (TBA) were acquired from Fuyu Fine Chemical Co., Ltd. (Tianjin, China). Ultrapure water was applied in all experiments.

2.2. Preparation of benzene and K^+ co-doped $g\text{-C}_3\text{N}_4$ (KBCN)

First, 3 g of MA and a certain amount of ATA (0, 20, 30, 40, or 60 mg) were added into 40 mL of deionized water, followed by stirring for 2 h at room temperature. The reaction mixture was sealed in a 100-mL Teflon-lined stainless-steel autoclave and stored at 180 C for 12 h, as shown in Fig. S2. The obtained MA–ATA powder was washed with deionized water, dried at 60 C, then placed in a covered ceramic crucible, heated to 550 C at a heating rate of 2 C min⁻¹ in a muffle furnace, and kept at 550 C for 4 h to obtain benzene-doped CN (BCN). Secondly, 0.60 g BCN was mixed with KCl (3.3 g) and LiCl (2.7 g) by grinding, followed by calcination at 550 C for 4 h under N₂ atmosphere. After cooling to room temperature, the prepared materials were washed with water and dried under vacuum. The obtained sample was denoted as KBCN. PCN was also prepared by the direct calcination of MA at 550 C for 4 h in a

1 muffle furnace. K⁺ doped CN (KCN) was obtained by the same method used for the
2
3 preparation of KBCN, but without the addition of ATA.
4
5

6 *2.3. Fenton-like degradation of RhB and CR*

7
8

9 In a typical experiment, 10 mg of photocatalyst was added to 50 mL of RhB or CR
10
11 (10 mg L⁻¹) aqueous solution, bubbled with O₂ for 30 min. Then, the suspension was
12
13 stirred for another 30 min in dark. Afterwards, the Fenton-like reaction was carried
14
15 out under a 300W xenon lamp irradiation ($\lambda > 420$ nm) for 1 h (PLS-SXE 300,
16
17 Beijing PerfectLight, China). The residual concentration of RhB and CR in the
18
19 supernatant was determined by an absorbance at 554 nm and 315 nm, respectively
20
21 using a UV-visible spectrophotometer (Shimadzu UV-2000). The degradation
22
23 experiments were measured three times, and the arithmetic means were reported. To
24
25 evaluate the recyclability of the photocatalyst, the sample was collected by
26
27 centrifugation and washed with deionized water and dried before use in the next
28
29 degradation experiments.
30
31
32
33
34
35
36
37
38
39
40
41

42 **3. Results and discussion**

43

44 *3.1. Structure characterization*

45
46

47 Fig. 1a displays the XRD patterns of PCN, BCN, KCN, and KBCN. The XRD
48
49 pattern of PCN exhibited two diffraction peaks at 27.40° and 13.04°, which could be
50
51 attributed to the (002) interplanar stacking of the conjugated aromatic system and the
52
53 (100) in-plane orientation of periodic tri-s-triazine units, respectively [41]. The XRD
54
55 pattern of BCN was similar to that of PCN, indicating that the main structure and
56
57
58
59
60
61
62
63
64
65

1 periodicity of CN were not damaged after introduction of ATA. In contrast, the
2
3 structure changed significantly after post-calcination in the LiCl–KCl mixture, as
4
5
6 evidenced by the XRD patterns of KCN and KBCN. The peak of the (100) plane
7
8
9 shifted to a lower diffraction degree of 8.20° , indicating an enlarged in-plane
10
11
12 periodicity, which was due to the incorporation of K^+ with a larger atomic size than C
13
14 and N between the triazine units [42]. Another peak of the (002) plane was centered at
15
16
17 28.20° , corresponding to a shift to higher angle compared to PCN. This suggested a
18
19
20 decreased interlayer distance due to the enhanced interaction among the layers in
21
22
23 KCN and KBCN, which might enable the transfer of electrons from K^+ to CN [43].
24
25
26 The other weak peaks in the XRD patterns of KCN and KBCN were assigned to the
27
28
29 formed poly(triazine imide) (PTI) [44].
30

31 [Figure 1]

32
33
34 The chemical structure of the synthesized samples was also determined by Fourier
35
36 transform infrared (FTIR) spectroscopy (Fig. 1b) and X-ray photoelectron
37
38 spectroscopy (XPS) measurements. The FTIR absorption band at 807 cm^{-1} was
39
40
41 ascribed to the out-of-plane bending vibration of heptazine; the peak at 913 cm^{-1} was
42
43
44 attributed to the bending vibration of the extended conjugated CN network with
45
46
47 tri-s-triazine units [45]; and the peaks in the range of $1200\text{--}1700\text{ cm}^{-1}$ were assigned
48
49
50 to the carbon and nitrogen heterocycles (Fig. 1b). Compared to PCN, BCN displayed
51
52
53 new peak at 730 cm^{-1} , corresponding to the C-H out-of-plane bending vibration of
54
55
56 aromatic ring, and peaks at 2850 and 2918 cm^{-1} can be assigned to the symmetric and
57
58
59 asymmetric stretching of the $-\text{CH}$ group, respectively. After post-calcination of PCN
60
61
62
63
64
65

1 and BCN with the LiCl–KCl mixture, new strong peaks appeared at 1000 and 2181
2
3 cm^{-1} . The former was assigned to the stretching vibration of oxygen-containing
4
5 groups (C–O) [45], indicating that hydroxyl groups, which might be caused by the
6
7 enlarged specific surface area [46] were present in KCN and KBCN. The latter was
8
9 attributed to the vibration of the $\text{C}\equiv\text{N}$ triple bond, probably stemming from the
10
11 decomposition of C–N rings during the remodeling process [41]. Compared to KCN,
12
13 peak of 1553 cm^{-1} become prominent and peak of 1454 cm^{-1} shifted to 1459 cm^{-1} due
14
15 to the embedding of the benzene ring by substituting some of the NH_2 groups of the
16
17 melem framework [33]. Benzene doping was further confirmed by solid-state ^{13}C
18
19 NMR (Fig. 1c). Compared to the ^{13}C NMR spectrum of KCN, weak peak appeared at
20
21 135 ppm in the ^{13}C NMR spectrum of KBCN and could be attributed to the aromatic
22
23 carbon structure [47], directly proving the presence of benzene in KBCN.
24
25
26
27
28
29
30
31
32

33
34 Fig. 2 shows the high-resolution XPS spectra of corresponding elements in PCN
35
36 and KBCN. In the $\text{C}1\text{s}$ spectrum, the distinct peaks at 284.7 and 288.1 eV correspond
37
38 to carbon contamination and $\text{N}-\text{C}=\text{N}$ ($\text{C}_{2\text{N}}$) in heptazine heterocyclic units,
39
40 respectively. For KBCN, a new peak appeared at 286.5 eV, which was assigned to the
41
42 C–OH [48] and C– NH_x on the edges of heptazine units [34] groups, confirming the
43
44 FTIR results. The $\text{N}1\text{s}$ spectrum shown in Fig. 2b could be deconvoluted into four
45
46 peaks at 398.5, 399.9, 400.7, and 403.5 eV, which were related to C–N=C ($\text{N}_{2\text{C}}$),
47
48 N–(C) $_3$ ($\text{N}_{3\text{C}}$), N–H (NH_x), and π excitations, respectively. Table S1 lists the areas of
49
50 the $\text{N}1\text{s}$ XPS fitting peaks. The relative content of N in the NH_x groups decreased
51
52 from 0.182 (PCN) to 0.179 (KBCN; Table S1), which could be ascribed to the
53
54
55
56
57
58
59
60
61
62
63
64
65

1 presence of $\text{CN}\equiv$ groups, as they bind to similar C functional groups as $-\text{NH}_x$, or to
2
3 the interaction between $-\text{NH}-$ and K^+ [41]. Moreover, the peak area ratio of $\text{N}_{3\text{C}}$ to $\text{N}_{2\text{C}}$
4
5 decreased from 0.81 for PCN to 0.49 for KBCN, indicating that more $\text{N}_{2\text{C}}$ was formed
6
7 after incorporation of benzene [49]. The $\text{O}1\text{s}$ spectrum of KBCN revealed three peaks
8
9 at 532.9, 532.0, and 530.9 eV, corresponding to C–O, surface-adsorbed oxygen/O–H
10
11 [50], and N–C–O [45], respectively. The $\text{K}2\text{p}$ spectrum in Fig. 2d displays two peaks
12
13 at 295.3 and 292.6 eV, which are characteristic of the binding energies of K^+ ions,
14
15 indicating that K^+ ions were integrated into the framework of the KCN and KBCN
16
17 structures [46]. Additionally, the atomic ratios of C and O in KBCN obtained by XPS
18
19 analysis are higher than those values in PCN (Table S2). Thus, these results indicated
20
21 that benzene and K^+ were successfully co-incorporated into the framework of CN.
22
23
24
25
26
27
28
29
30

31 [Figure 2]

32
33 The morphology of as-prepared KBCN catalyst was observed by SEM and TEM.
34
35 PCN has an aggregated layered structure (Fig. S3), while KBCN exhibited a strip-like
36
37 structure. Moreover, a crystal lattice constant of 1.01 nm was observed in its
38
39 high-resolution transmission electron microscopy (HRTEM) image, which is
40
41 indicative of the (100) in-plane orientation, showing that KBCN was highly
42
43 crystalline (Fig. S4) [39]. High-angle annular dark-field scanning transmission
44
45 electron microscopy (HAADF–STEM) and energy-dispersive X-ray spectroscopy
46
47 (EDS) elemental mapping imaging further showed that C, N, K, and O were
48
49 homogeneously distributed in strip-like KBCN. Moreover, KBCN has a higher S_{BET}
50
51 value ($44.2 \text{ m}^2 \text{ g}^{-1}$) compared to BCN ($6.02 \text{ m}^2 \text{ g}^{-1}$), and has micropores and
52
53
54
55
56
57
58
59
60
61
62
63
64
65

mesopores as evidenced by the BJH pore size distribution curve (Fig. S5).

[Figure 3]

The optical properties and band structures of the prepared samples were analyzed by UV–Vis diffuse reflectance spectroscopy (UV–Vis DRS). As shown in Fig. 4a, PCN exhibited a low visible light absorption with the adsorption edge at around 460 nm. The absorption band tail slightly increased in the visible region after introduction of ATA into CN (BCN), indicating the presence of n- π^* electron transition in BCN [33,51]. Both the ultraviolet and visible light absorption capacities were largely enhanced after K⁺ intercalation into PCN and BCN, and the light absorption ability of KCN was slightly stronger than that of KBCN. The extended light absorption of the composites is also consistent with their color changes (Fig. S6). Furthermore, the band gap potentials (E_g) of the prepared samples were determined, revealing values of 2.76, 2.78, 2.74, and 2.71 eV for PCN, BCN, KCN, and KBCN, respectively (Fig. S7). In addition, according to the VB–XPS plots (Fig. S8), the VB potentials were 1.82, 1.74, 1.78, and 1.67 eV for PCN, BCN, KCN, and KBCN, respectively. Thus, the CB potentials were determined using the formula $E_{CB} = E_{VB} - E_g$ (Fig. S9).

3.2. Photocatalytic H₂O₂ production

Because the degradation was achieved by in situ-generated H₂O₂, the ability of obtained samples to generate H₂O₂ was first evaluated. As shown in Fig. 4b, the performance of PCN was poor, as only 2.60 μ M H₂O₂ was produced after 60 min visible light irradiation in pure water. The amount of produced H₂O₂ slightly increased to 3.89 μ M over BCN obtained by calcination of the assembly of MA and

1 40 mg ATA (Fig. S10). However, the samples that were prepared via post-calcination
2
3 with LiCl–KCl displayed greatly enhanced H₂O₂ production activity. The
4
5 concentration of H₂O₂ produced over KCN reached 22.2 μM after 60 min irradiation,
6
7
8 which further increased to 57.7 μM for KBCN. This value was 22.0 times larger than
9
10 that for PCN.
11

12
13
14 During the photocatalytic H₂O₂ production, decomposition of H₂O₂ simultaneously
15
16 occurred by photogenerated electrons to produce ·OH, which will participate in
17
18 Fenton-like degradation reaction. To better understand the degradation performance of
19
20 obtained sample, the decomposition of H₂O₂ was investigated by subjecting 1 mM
21
22 H₂O₂ solution to light illumination in the presence of the prepared samples. As shown
23
24 in Fig. 4c, the H₂O₂ decomposition rates followed an order of PCN < BCN < KBCN <
25
26 KCN. More H₂O₂ was decomposed over KBCN, which could be beneficial for
27
28 Fenton-like degradation. Furthermore, the H₂O₂ production kinetics were evaluated
29
30 based on zero-order kinetics (H₂O₂ formation, [H₂O₂] = k_f/k_d (1–exp(–k_d t)) and
31
32 first-order kinetics (H₂O₂ decomposition, k_d = –dC_t/dt; Fig. S11). KBCN has the
33
34 higher formation (k_f) (0.0485 μmol min^{–1}) and decomposition (k_d) (0.0128 min^{–1})
35
36 values. This suggested that the H₂O₂ formation and decomposition reactions were
37
38 accelerated under activation of KBCN.
39
40
41
42
43
44
45
46
47
48
49

50 **[Figure 4]**

51 3.3. Fenton-like degradation of RhB and CR

52
53 The ability of the obtained sample to degrade RhB and CR was investigated at
54
55 natural pH and without addition of Fe²⁺ species. As shown in Fig. 5a,c, KBCN
56
57
58
59
60
61
62
63
64
65

1 exhibited the highest activity in the degradation of RhB and CR among all samples, as
2
3 93.3% RhB and 96.6% CR were degraded after 60 min irradiation. Under the same
4
5 conditions, only 48.7%, 75.8%, and 82.2% of RhB, as well as 75.5%, 84.1%, and 91.0%
6
7 CR were removed by PCN, BCN, and KCN, respectively. The RhB and CR
8
9 degradation efficiency follows the same orders as those H₂O₂ yield, implying that the
10
11 enhanced H₂O₂ production played an important roles in the RhB and CR degradation.
12
13 The removal of RhB and CR over PCN mainly attributed to its absorption capability.
14
15 Furthermore, the degradation kinetics of RhB and CR were described by fitting the
16
17 first-order kinetics equation. The apparent rate constants (*k*) of RhB and CR for
18
19 KBCN are 0.0446 and 0.0497 min⁻¹ (Fig. S12), which are 4.1 and 2.5 times higher
20
21 than those of PCN (0.0107 and 0.0200 min⁻¹, respectively).
22
23
24
25
26
27
28
29
30

31 [Figure 5]

32
33 The recycle experiments were performed to study the stability of KBCN for H₂O₂
34
35 production and Fenton-like degradation. First, the H₂O₂ production over KBCN was
36
37 repeated for up to five cycles under the same condition (Fig. 4d). After five test cycles,
38
39 the amount of produced H₂O₂ slightly decreased to 56.0 μM. Moreover, the XRD
40
41 pattern of used KBCN was similar to that of the fresh sample (Fig. S13), suggesting
42
43 that the KBCN catalyst was stable and reusable. Then the Fenton-like degradation of
44
45 RhB and CR over KBCN using in situ-generated H₂O₂ was repeated. 92.1% RhB and
46
47 93.1% CR still can be removed after four cycles of testing (Fig. 5b,d), demonstrating
48
49 that KBCN has good durability in Fenton-like degradation.
50
51
52
53
54
55
56
57

58 3.4. Mechanism studies

59
60
61
62
63
64
65

3.4.1. Mechanism for enhanced H₂O₂ production

Compared to PCN and BCN, KCN and KTCN show significant improved H₂O₂ production (Fig. 5) but negligible changes in band positions. This indicates that the enhanced H₂O₂ production cannot be explained by their changed band positions. To explain highly enhanced H₂O₂ production over KBCN, the charge separation performances of obtained samples were first evaluated by electrochemical measurements (Fig. S14). KBCN exhibits slightly weaker PL intensities, has the highest photocurrent and the smallest EIS Nyquist plot semicircle compared to PCN, BCN, and KCN, indicating that molten salt treatment can suppress charge recombination, benzene and K⁺ co-doping could more efficiently promote the separation and transfer of electron-hole pairs of CN. In addition, the Kohn–Sham orbitals of KCN and KBCN were constructed by Gaussian calculation to analyze their electron distribution (Fig. S15). As shown in Fig. 6a, The LUMO of KCN exhibited π and π^* characteristics arising from the contributions of C 2p and N 2p orbitals, which is in agreement with a previous report [43]. The HOMOs were not located on the same tri-s-triazine rings (Fig. 6b), indicating that K⁺ doping was beneficial for the separation of photogenerated charge carriers. However, the electrons of KBCN were redistributed due to benzene doping. As shown in Fig. 6c, the LUMO of KBCN was dominated by a bridging benzene and two tri-s-triazine rings, whereas the HOMO was mainly distributed over the benzene moiety and other tri-s-triazine rings (Fig. 6d). These separated frontier orbitals were conducive to the spatial separation of photogenerated charge carriers [49]. Therefore, the inserted benzene could act as a

1 bridge to facilitate spatial electron transfer in tri-s-triazine, resulting in charge
2
3 rearrangement and enhanced charge separation.
4

6 [Figure 6]

7
8
9 Control sample of KBCN_{4h} obtained by soaking KBCN in 80°C water for 4 h to
10
11 remove K⁺ were prepared [25], and the yield of H₂O₂ over KBCN_{4h} is 51.2 μM in 60
12
13 min (Fig. S16), lower than that for KBCN (57.7 μM). Thus, combination the
14
15 negligible changes in band positions and high charge separation efficiency of KBCN,
16
17 we assume that the high H₂O₂ production activity resulted from the synergistic effects
18
19 of the benzene and K⁺ dopants. First, K⁺ doping by recalcination in LiCl–KCl
20
21 increases the light absorption, diminishes the defects that could induce charge carries
22
23 recombination. Second, positive charged K⁺ can act as Lewis acidic sites for
24
25 facilitating oxidation of water, as well as enhance the capability of O₂ [25]. Third, the
26
27 doped benzene could act as the bridging N atoms for reducing the symmetry of the
28
29 tri-s-triazine ring of CN, promotes electrons-holes separation, resulting in more
30
31 electrons participating in O₂ reduction.
32
33
34
35
36
37
38
39
40

41 3.4.2. Possible mechanism for Fenton-like degradation with in situ-generated H₂O₂

42
43
44 The mechanism was elucidated from two aspects. One was the photocatalytic H₂O₂
45
46 production, and the other was the Fenton-like degradation of RhB and CR. First, 5,
47
48 5-dimethyl-1-pyrrolidine N-oxide (DMPO) spin-trapping electron paramagnetic
49
50 resonance (EPR) technique was employed to measure whether ·O₂⁻ had been
51
52 generated. As shown in Fig. 7c, the characteristic peaks of DMPO–O₂⁻ were detected
53
54 for KBCN after 3 min irradiation, and the H₂O₂ concentration suddenly decreased to
55
56
57
58
59
60
61
62
63
64
65

1 5.7 μM in the presence of the $\cdot\text{O}_2^-$ scavenger BQ (Fig. S18a), confirming the presence
2
3 of $\cdot\text{O}_2^-$ during H_2O_2 production. In addition, Koutecky–Levich plots (Figs. S 17 and
4
5
6 18b) confirm that the number of electrons (n_e) which takes part in the reduction of O_2
7
8
9 are 1.21, 1.31, 1.24, and 1.33 for PCN, BCN, KCN, and KBCN, respectively. Thus, it
10
11 can be concluded that single-electron two-step reduction route dominate the H_2O_2
12
13 production process ($\text{O}_2 + e^- \rightarrow \cdot\text{O}_2^-$ and $\cdot\text{O}_2^- + 2\text{H}^+ + e^- \rightarrow \text{H}_2\text{O}_2$) but a two-electron
14
15 one-step reduction route also exist ($\text{O}_2 + 2\text{H}^+ + 2e^- \rightarrow \text{H}_2\text{O}_2$) [51].
16
17
18
19

20 To reveal the mechanism for Fenton-like degradation of RhB and CR, the
21
22 degradation tests over KBCN in the presence of $\cdot\text{OH}$ scavenger of TBA were
23
24 conducted (Fig. 7a,b). Compared to the blank sample, the RhB and CR degradation
25
26 efficiency significantly decreased, proving that $\cdot\text{OH}$ was the active species to degrade
27
28 RhB and CR. In addition, the degradation tests were carried out under N_2 atmosphere,
29
30
31 and merely 28.4% RhB and 32.4% CR were degraded after 60 min irradiation. Similar
32
33 suddenly decreased degradation efficiency was observed in the presence of BQ.
34
35 Under N_2 atmosphere or with BQ, little H_2O_2 was produced (Fig. S18a), which means
36
37 that little $\cdot\text{OH}$ was evolved and consequently the degradation efficiency of RhB and
38
39 CR greatly decreased. Furthermore, TA photoluminescence probing technique (TA-PL)
40
41 was employed to confirm the generation of $\cdot\text{OH}$ radicals in KBCN [5]. TA can trap
42
43 the $\cdot\text{OH}$ radicals to form fluorescent 2-hydroxy terephthalic acid (HTA), which has a
44
45 PL emission peak at 426 nm. Then, the PL intensities of the KBCN/TA system at
46
47 different irradiation time were investigated. As shown in Fig. 7d, the PL intensity
48
49 gradual increased with irradiation time, suggesting the formation of $\cdot\text{OH}$ radicals in
50
51
52
53
54
55
56
57
58
59
60
61
62
63
64
65

1 KBCN. Thus, all above results proved that efficient degradation of RhB and CR
2
3 comes from the oxidization of $\cdot\text{OH}$ which derived from in situ-generated H_2O_2 .
4
5

6 [Figure 7]

7
8 A possible mechanism for photocatalytic RhB and CR degradation via a
9 Fenton-like reaction over KBCN with in situ-generated H_2O_2 production is proposed
10 (Fig. 8). Initially, upon illumination, electron and holes are generated, and then
11 separate and transfer to the surface, where the holes oxidize water under the help of
12 doped K^+ ion²⁵ and release the protons for H_2O_2 production; Simultaneously, O_2
13 molecules is reduced by electrons to form $\cdot\text{O}_2^-$. After that, the released H^+ reacts with
14 $\cdot\text{O}_2^-$ to generate H_2O_2 . Subsequently, the produced H_2O_2 was reduced to $\cdot\text{OH}$ radicals,
15
16 which then oxidize the RhB and CR.
17
18
19
20
21
22
23
24
25
26
27
28
29
30

31 [Figure 8]

32
33 The formed intermediate products and degradation pathways of RhB and CR over
34 KBCN were further analyzed by liquid chromatography-mass spectrometry (LC-MS).
35
36 As shown in Figs. S19 and 9, degradation of CR occurred via cleavage of two
37 sulfonate groups [52], leading to the formation of m/z 491 and 475, which could
38 transformed into m/z 473. Then, m/z 301, 267, 258, 249, 226, 222, 199 and 197 were
39 formed via cleavage of azo ($-\text{N}=\text{N}-$) double bond, C-C and C-N bonds. The
40 oxidation products of m/z 289, 208, 46 were further formed under actions of $\cdot\text{OH}$. For
41 RhB degradation process (Figs. S20 and 10), first, one of ethyl groups of
42 ethylethanaminium in RhB (m/z 443) was removed from RhB to form m/z 415 [53].
43
44
45
46
47
48
49
50
51
52
53
54
55
56
57
58
59
60
61
62
63
64
65

1 304 and 288 were formed by oxidization of carboxyphenyl group, and m/z 182 was
2
3 transformed into m/z 132 through the ring-opening, which was then transformed into
4
5 low-molecular-weight compounds of m/z 104, 102, 86, 74 and 62.
6
7

8
9 **[Figure 9]**

10
11 **[Figure 10]**

12 13 14 **4. Conclusions**

15
16
17 Highly efficient benzene and K^+ co-doped CN was successfully prepared by
18
19 thermal polymerization of an assembly of melamine and 2-aminoterephthalic acid,
20
21 followed by post-calcination with LiCl–KCl molten salt, which then used to degrade
22
23 RhB and CR via Fenton-like reaction with in situ-generated H_2O_2 . KBCN can
24
25 produce 57.7 μM H_2O_2 in pure water after 60 min irradiation. It also exhibits high
26
27 H_2O_2 decomposition rate. Consequently, KBCN could degrade 93.3% RhB and 96.6%
28
29 CR after 60 min with H_2O_2 -derived $\cdot OH$ radicals at natural pH, which were higher
30
31 than those of PCN (48.7% and 75.5%, respectively). KBCN also exhibited excellent
32
33 stability and recyclability of H_2O_2 production, RhB and CR degradation. The
34
35 enhanced performance was mainly due to the synergy effects of benzene and K^+
36
37 dopants, and efficient charge carriers separation. This work demonstrates an efficient
38
39 approach to modify CN for efficient production of H_2O_2 and degradation of dyes.
40
41
42
43
44
45
46
47
48
49
50
51
52

53 **Acknowledgements**

54
55
56 The authors acknowledge funding support from the National Natural Science
57
58 Foundation of China (52171140, 51772162 and 52072197), Outstanding Youth
59
60
61
62
63
64
65

1 Foundation of Shandong Province, China (ZR2019JQ14), Youth Innovation and
2
3 Technology Foundation of Shandong Higher Education Institutions, China
4
5 (2019KJC004), Major Scientific and Technological Innovation Project
6
7 (2019JZZY020405), Major Basic Research Program of Natural Science Foundation of
8
9 Shandong Province under Grant (ZR2020ZD09), and Taishan Scholar Young Talent
10
11 Program (tsqn201909114).
12
13
14
15
16
17
18
19
20

21 **References**

- 22
23
24 [1] Yin HF, Cao Y, Fan TL, Li PF, Chen SM, Liu XH. Construction of
25
26 FEOOH/semiconductor nanosheets heterogeneous catalysts for efficient
27
28 photo-Fenton degradation of tetracycline hydrochloride. *J Taiwan Ins Chem E*
29
30 2021;119:70–9.
31
32
33
34 [2] Liu Y, Zhao Y, Wang JL. Fenton/Fenton-like processes with in-situ production of
35
36 hydrogen peroxide/hydroxyl radical for degradation of emerging contaminants:
37
38 Advances and prospects. *J Hazard Mater* 2021;404:124191–210.
39
40
41
42 [3] Meng WD, Wang YP, ZhangYT, Liu C, Wang ZB, Song ZL, Xu BB, Qi F, Ikhlaq A.
43
44 Degradation Rhodamine B dye wastewater by sulfate radical-based visible light-fenton
45
46 mediated by LaFeO₃: Reaction mechanism and empirical modeling. *J Taiwan Ins Chem*
47
48 E 2020;111:162–9.
49
50
51
52 [4] Nguyen CH, Tran ML, Van Tran TT, Juang RS. Efficient removal of antibiotic
53
54 oxytetracycline from water by Fenton-like reactions using reduced graphene
55
56
57
58
59
60
61
62
63
64
65

oxide-supported bimetallic Pd/nZVI nanocomposites. *J Taiwan Ins Chem E* 2021;119:80–9.

[5] Jiang ZY, Wang LZ, Lei JY, Liu YD, Zhang JL. Photo-Fenton degradation of phenol by CdS/rGO/Fe²⁺ at natural pH with in situ-generated H₂O₂. *Appl Catal B Environ* 2019;241:367–74.

[6] Bai XY, Li Y, Xie LB, Liu XH, Zhan SH, Hu WP. A novel Fe-free photo-electro-Fenton-like system for enhanced ciprofloxacin degradation: bifunctional Z-scheme WO₃/g-C₃N₄. *Environ Sci Nano* 2019;6:2850–62.

[7] Yang JR, Zeng DQ, Li J, Dong LQ, Ong WJ, He YL. A highly efficient Fenton-like catalyst based on isolated diatomic Fe-Co anchored on N-doped porous carbon. *Chem Eng J* 2021;404:126376–86.

[8] Jia XW, Sun F, Fei Y, Jin MP, Zhang F, Xu W, Shi N, Lv ZG. Explosion characteristics of mixtures containing hydrogen peroxide and working solution in the anthraquinone route to hydrogen peroxide. *Process Saf Environ Prot* 2018;119:218–22.

[9] Dong K, Lei Y, Zhao HT, Liang J, Ding P, Liu Q, Xu ZQ, Lu SY, Li Q, Sun XP. Noble-metal-free electrocatalysts toward H₂O₂ production. *J Mater Chem A* 2020;8:23123–41.

[10] Shiraishi Y, Takii T, Hagi T, Mori S, Kofuji Y, Kitagawa Y, Tanaka S, Ichikawa S, Hirai T. Resorcinol-formaldehyde resins as metal-free semiconductor photocatalysts for solar-to-hydrogen peroxide energy conversion. *Nat Mater* 2019;18:985–93.

- 1 [11] Freakley SJ, He Q, Harrhy JH, Lu L, Crole DA, Morgan DJ, Ntainjua EN,
2
3 Edwards JK, Carley AF, Borisevich AY, Kiely CJ, Hutchings GJ. Palladium-tin
4
5 catalysts for the direct synthesis of H₂O₂ with high selectivity. Science
6
7
8
9 2016;351:965–8.
- 10
11 [12] Zhang P, Sun DR, Cho A, Weon S, Lee S, Lee J, Han JW, Kim DP, Choi W.
12
13 Modified carbon nitride nanozyme as bifunctional glucose oxidase-peroxidase for
14
15 metal-free bioinspired cascade photocatalysis. Nat Commun 2019;10: 940–53.
16
17
18
19
- 20 [13] Gogoi S, Karak N. Solar-driven hydrogen peroxide production using
21
22 polymer-supported carbon dots as heterogeneous catalyst. Nano-micro Lett
23
24
25 2017;9:40–50.
26
27
- 28 [14] Hu JD, Chen C, Hu T, Li JS, Lu H, Zheng Y, Yang XG, Guo CX, Li CM.
29
30 Metal-free heterojunction of black phosphorus/oxygen-enriched porous g-C₃N₄ as
31
32 an efficient photocatalyst for Fenton-like cascade water purification. J Mater
33
34
35 Chem A 2020;8:19484–92.
36
37
38
- 39 [15] Chen L, Xie YX, Yu CG, Huang RY, Du QY, Zhao JW, Sun WZ, Wang WW.
40
41 Enhanced Fenton-like catalytic activity and stability of g-C₃N₄ nanosheet-wrapped
42
43 copper phosphide with strong anti-interference ability: Kinetics and mechanistic
44
45 study. J Colloid Interf Sci 2021;595:129–41.
46
47
48
49
- 50 [16] Wang YB, Meng D, Zhao X. Visible-light-driven H₂O₂ production from O₂
51
52 reduction with nitrogen vacancy-rich and porous graphitic carbon nitride. Appl
53
54
55 Catal B Environ 2020;273:119064–72.
56
57
58
59
60
61
62
63
64
65

- 1 [17] Chen X, Zhang WW, Zhang LX, Feng LP, Zhang CX, Jiang J, Yan TJ, Wang H.
2
3 Sacrificial agent-free photocatalytic H₂O₂ evolution via two-electron oxygen
4 reduction using a ternary a-Fe₂O₃/CQD@g-C₃N₄ photocatalyst with
5
6 broad-spectrum response. *J Mater Chem A* 2020;8:18816–25.
7
8
9
10
11 [18] Liu Y, Zhao YJ, Wu QY, Wang X, Nie HD, Zhou YJ, Huang H, Shao MW, Liu
12 Y, Kang ZH. Charge storage of carbon dot enhances photo-production of H₂ and
13 H₂O₂ over Ni₂P/carbon dot catalyst under normal pressure. *Chem Eng J*
14 2021;409:128184–91.
15
16
17
18
19
20
21
22 [19] Zhao YJ, Liu Y, Cao JJ, Wang H, Shao MW, Huang H, Liu Y, Kang ZH. Efficient
23 production of H₂O₂ via two-channel pathway over ZIF-8/g-C₃N₄ composite
24 photocatalyst without any sacrificial agent. *Appl Catal B: Environ*
25 2020;278:119289–95.
26
27
28
29
30
31
32
33 [20] Chen YM, Gu WQ, Tan L, Ao ZM, An TC, Wang SB. Photocatalytic H₂O₂
34 production using Ti₃C₂ MXene as a non-noble metal cocatalyst. *Appl Catal A Gen*
35 2021;618:118127–33.
36
37
38
39
40
41
42 [21] Dang XM, Yang RY, Wang Z, Wu SY, Zhao HM. Efficient visible-light activation
43 of molecular oxygen to produce hydrogen peroxide using P doped g-C₃N₄ hollow
44 spheres. *J Mater Chem A* 2020;8:22720–7.
45
46
47
48
49
50 [22] Hou HL, Zeng XK, Zhang XW. Production of hydrogen peroxide through
51 photocatalytic processes: A critical review of recent advances. *Angew Chem Int*
52 Ed 2020;59:17356–76.
53
54
55
56
57
58 [23] Wei Z, Liu ML, Zhang ZJ, Yao WQ, Tan HW, Zhu YF. Efficient
59
60
61
62
63
64
65

1 visible-light-driven selective oxygen reduction to hydrogen peroxide by
2
3 oxygen-enriched graphitic carbon nitride polymers. *Energy Environ Sci*
4
5
6 2018;11:2581–9.
7

8
9 [24] Moon GH, Fujitsuka M, Kim S, Majima T, Wang XC, Choi W. Eco-friendly
10
11 photochemical production of H₂O₂ through O₂ reduction over carbon nitride
12
13 frameworks incorporated with multiple heteroelements. *ACS Catal* 2017;7:2886–
14
15 95.
16
17

18
19 [25] Zhang JZ, Yu CY, Lang JY, Zhou YF, Zhou BX, Hu YH, Long M. Modulation of
20
21 lewis acidic-basic sites for efficient photocatalytic H₂O₂ production over
22
23 potassium intercalated tri-s-triazine materials. *Appl Catal B Environ*
24
25 2020;277:119225–33.
26
27

28
29 [26] Shiraishi Y, Kanazawa S, Kofuji Y, Sakamoto H, Ichikawa S, Tanaka S, Hirai T.
30
31 Sunlight-driven hydrogen peroxide production from water and molecular oxygen
32
33 by metal-free photocatalysts. *Angew Chem Int Ed* 2014;53 :13454–9.
34
35
36

37
38 [27] He F, Wang ZX, Li YX, Peng SQ, Liu B. The nonmetal modulation of
39
40 composition and morphology of g-C₃N₄-based Photocatalysts. *Appl Catal B*
41
42 *Environ* 2020;269:118828–48.
43
44
45

46
47 [28] Teng ZY, Cai WN, Liu SX, Wang CY, Zhang QT, Su CL, Ohno T. Bandgap
48
49 engineering of polymetric carbon nitride copolymerized by 2,5,8-
50
51 triamino-tri-s-triazine (melem) and barbituric acid for efficient nonsacrificial
52
53 photocatalytic H₂O₂ production. *Appl Catal B Environ* 2020;271:118917–28.
54
55
56

57
58 [29] Li YH, Gu ML, Zhang XM, Fan JJ, Lv KL, Carabineiro SAC, Dong F. 2D
59
60
61
62
63
64
65

1 g-C₃N₄ for advancement of photogenerated carrier dynamics: Status and
2
3 challenges. Mater Today 2020;41:270–303.
4
5

6 [30] Liang L, Shi L, Wang FX, Wang HH, Yan PQ, Cong YF, Yao LZ, Yang ZX, Qi W.

7
8 g-C₃N₄ nano-fragments as highly efficient hydrogen evolution photocatalysts:
9 Boosting effect of nitrogen vacancy. Appl Catal A Gen 2020;599:117618–27.
10
11
12

13 [31] Yu Y, Yan W, Gao WY, Li P, Wang XF, Wu SM, Song WG, Ding KJ. Aromatic

14 ring substituted g-C₃N₄ for enhanced photocatalytic hydrogen evolution. J Mater
15
16
17
18
19
20
21
22 Chem A 2017;5:17199–203.

23 [32] Cao JJ, Wu QY, Zhao YJ, Wei KQ, Li Y, Wang X, Liao F, Huang H, Shao MW,

24
25 Liu Y, Kang ZH. In-situ photovoltage transients assisted catalytic study on H₂O₂
26
27
28
29
30
31
32 photoproduction over organic molecules modified carbon nitride photocatalyst.
33
34
35
36
37
38
39
40
41
42
43
44
45
46
47
48
49
50
51
52
53
54
55
56
57
58
59
60
61
62
63
64
65
66
67
68
69
70
71
72
73
74
75
76
77
78
79
80
81
82
83
84
85
86
87
88
89
90
91
92
93
94
95
96
97
98
99
100
101
102
103
104
105
106
107
108
109
110
111
112
113
114
115
116
117
118
119
120
121
122
123
124
125
126
127
128
129
130
131
132
133
134
135
136
137
138
139
140
141
142
143
144
145
146
147
148
149
150
151
152
153
154
155
156
157
158
159
160
161
162
163
164
165
166
167
168
169
170
171
172
173
174
175
176
177
178
179
180
181
182
183
184
185
186
187
188
189
190
191
192
193
194
195
196
197
198
199
200
201
202
203
204
205
206
207
208
209
210
211
212
213
214
215
216
217
218
219
220
221
222
223
224
225
226
227
228
229
230
231
232
233
234
235
236
237
238
239
240
241
242
243
244
245
246
247
248
249
250
251
252
253
254
255
256
257
258
259
260
261
262
263
264
265
266
267
268
269
270
271
272
273
274
275
276
277
278
279
280
281
282
283
284
285
286
287
288
289
290
291
292
293
294
295
296
297
298
299
300
301
302
303
304
305
306
307
308
309
310
311
312
313
314
315
316
317
318
319
320
321
322
323
324
325
326
327
328
329
330
331
332
333
334
335
336
337
338
339
340
341
342
343
344
345
346
347
348
349
350
351
352
353
354
355
356
357
358
359
360
361
362
363
364
365
366
367
368
369
370
371
372
373
374
375
376
377
378
379
380
381
382
383
384
385
386
387
388
389
390
391
392
393
394
395
396
397
398
399
400
401
402
403
404
405
406
407
408
409
410
411
412
413
414
415
416
417
418
419
420
421
422
423
424
425
426
427
428
429
430
431
432
433
434
435
436
437
438
439
440
441
442
443
444
445
446
447
448
449
450
451
452
453
454
455
456
457
458
459
460
461
462
463
464
465
466
467
468
469
470
471
472
473
474
475
476
477
478
479
480
481
482
483
484
485
486
487
488
489
490
491
492
493
494
495
496
497
498
499
500
501
502
503
504
505
506
507
508
509
510
511
512
513
514
515
516
517
518
519
520
521
522
523
524
525
526
527
528
529
530
531
532
533
534
535
536
537
538
539
540
541
542
543
544
545
546
547
548
549
550
551
552
553
554
555
556
557
558
559
560
561
562
563
564
565
566
567
568
569
570
571
572
573
574
575
576
577
578
579
580
581
582
583
584
585
586
587
588
589
590
591
592
593
594
595
596
597
598
599
600
601
602
603
604
605
606
607
608
609
610
611
612
613
614
615
616
617
618
619
620
621
622
623
624
625
626
627
628
629
630
631
632
633
634
635
636
637
638
639
640
641
642
643
644
645
646
647
648
649
650
651
652
653
654
655
656
657
658
659
660
661
662
663
664
665
666
667
668
669
670
671
672
673
674
675
676
677
678
679
680
681
682
683
684
685
686
687
688
689
690
691
692
693
694
695
696
697
698
699
700
701
702
703
704
705
706
707
708
709
710
711
712
713
714
715
716
717
718
719
720
721
722
723
724
725
726
727
728
729
730
731
732
733
734
735
736
737
738
739
740
741
742
743
744
745
746
747
748
749
750
751
752
753
754
755
756
757
758
759
760
761
762
763
764
765
766
767
768
769
770
771
772
773
774
775
776
777
778
779
780
781
782
783
784
785
786
787
788
789
790
791
792
793
794
795
796
797
798
799
800
801
802
803
804
805
806
807
808
809
810
811
812
813
814
815
816
817
818
819
820
821
822
823
824
825
826
827
828
829
830
831
832
833
834
835
836
837
838
839
840
841
842
843
844
845
846
847
848
849
850
851
852
853
854
855
856
857
858
859
860
861
862
863
864
865
866
867
868
869
870
871
872
873
874
875
876
877
878
879
880
881
882
883
884
885
886
887
888
889
890
891
892
893
894
895
896
897
898
899
900
901
902
903
904
905
906
907
908
909
910
911
912
913
914
915
916
917
918
919
920
921
922
923
924
925
926
927
928
929
930
931
932
933
934
935
936
937
938
939
940
941
942
943
944
945
946
947
948
949
950
951
952
953
954
955
956
957
958
959
960
961
962
963
964
965
966
967
968
969
970
971
972
973
974
975
976
977
978
979
980
981
982
983
984
985
986
987
988
989
990
991
992
993
994
995
996
997
998
999
1000

10 [33] Jia GR, Wang Y, Cui XQ, Yang ZX, Liu LL, Zhan HY, Wu Q, Zheng LR, Zheng
11
12
13
14
15
16
17
18
19
20
21
22
23
24
25
26
27
28
29
30
31
32
33
34
35
36
37
38
39
40
41
42
43
44
45
46
47
48
49
50
51
52
53
54
55
56
57
58
59
60
61
62
63
64
65
66
67
68
69
70
71
72
73
74
75
76
77
78
79
80
81
82
83
84
85
86
87
88
89
90
91
92
93
94
95
96
97
98
99
100
101
102
103
104
105
106
107
108
109
110
111
112
113
114
115
116
117
118
119
120
121
122
123
124
125
126
127
128
129
130
131
132
133
134
135
136
137
138
139
140
141
142
143
144
145
146
147
148
149
150
151
152
153
154
155
156
157
158
159
160
161
162
163
164
165
166
167
168
169
170
171
172
173
174
175
176
177
178
179
180
181
182
183
184
185
186
187
188
189
190
191
192
193
194
195
196
197
198
199
200
201
202
203
204
205
206
207
208
209
210
211
212
213
214
215
216
217
218
219
220
221
222
223
224
225
226
227
228
229
230
231
232
233
234
235
236
237
238
239
240
241
242
243
244
245
246
247
248
249
250
251
252
253
254
255
256
257
258
259
260
261
262
263
264
265
266
267
268
269
270
271
272
273
274
275
276
277
278
279
280
281
282
283
284
285
286
287
288
289
290
291
292
293
294
295
296
297
298
299
300
301
302
303
304
305
306
307
308
309
310
311
312
313
314
315
316
317
318
319
320
321
322
323
324
325
326
327
328
329
330
331
332
333
334
335
336
337
338
339
340
341
342
343
344
345
346
347
348
349
350
351
352
353
354
355
356
357
358
359
360
361
362
363
364
365
366
367
368
369
370
371
372
373
374
375
376
377
378
379
380
381
382
383
384
385
386
387
388
389
390
391
392
393
394
395
396
397
398
399
400
401
402
403
404
405
406
407
408
409
410
411
412
413
414
415
416
417
418
419
420
421
422
423
424
425
426
427
428
429
430
431
432
433
434
435
436
437
438
439
440
441
442
443
444
445
446
447
448
449
450
451
452
453
454
455
456
457
458
459
460
461
462
463
464
465
466
467
468
469
470
471
472
473
474
475
476
477
478
479
480
481
482
483
484
485
486
487
488
489
490
491
492
493
494
495
496
497
498
499
500
501
502
503
504
505
506
507
508
509
510
511
512
513
514
515
516
517
518
519
520
521
522
523
524
525
526
527
528
529
530
531
532
533
534
535
536
537
538
539
540
541
542
543
544
545
546
547
548
549
550
551
552
553
554
555
556
557
558
559
560
561
562
563
564
565
566
567
568
569
570
571
572
573
574
575
576
577
578
579
580
581
582
583
584
585
586
587
588
589
590
591
592
593
594
595
596
597
598
599
600
601
602
603
604
605
606
607
608
609
610
611
612
613
614
615
616
617
618
619
620
621
622
623
624
625
626
627
628
629
630
631
632
633
634
635
636
637
638
639
640
641
642
643
644
645
646
647
648
649
650
651
652
653
654
655
656
657
658
659
660
661
662
663
664
665
666
667
668
669
670
671
672
673
674
675
676
677
678
679
680
681
682
683
684
685
686
687
688
689
690
691
692
693
694
695
696
697
698
699
700
701
702
703
704
705
706
707
708
709
710
711
712
713
714
715
716
717
718
719
720
721
722
723
724
725
726
727
728
729
730
731
732
733
734
735
736
737
738
739
740
741
742
743
744
745
746
747
748
749
750
751
752
753
754
755
756
757
758
759
760
761
762
763
764
765
766
767
768
769
770
771
772
773
774
775
776
777
778
779
780
781
782
783
784
785
786
787
788
789
790
791
792
793
794
795
796
797
798
799
800
801
802
803
804
805
806
807
808
809
810
811
812
813
814
815
816
817
818
819
820
821
822
823
824
825
826
827
828
829
830
831
832
833
834
835
836
837
838
839
840
841
842
843
844
845
846
847
848
849
850
851
852
853
854
855
856
857
858
859
860
861
862
863
864
865
866
867
868
869
870
871
872
873
874
875
876
877
878
879
880
881
882
883
884
885
886
887
888
889
890
891
892
893
894
895
896
897
898
899
900
901
902
903
904
905
906
907
908
909
910
911
912
913
914
915
916
917
918
919
920
921
922
923
924
925
926
927
928
929
930
931
932
933
934
935
936
937
938
939
940
941
942
943
944
945
946
947
948
949
950
951
952
953
954
955
956
957
958
959
960
961
962
963
964
965
966
967
968
969
970
971
972
973
974
975
976
977
978
979
980
981
982
983
984
985
986
987
988
989
990
991
992
993
994
995
996
997
998
999
1000

10 [34] Li SS, Peng YN, Hu C, Chen ZH. Self-assembled synthesis of

11
12
13
14
15
16
17
18
19
20
21
22
23
24
25
26
27
28
29
30
31
32
33
34
35
36
37
38
39
40
41
42
43
44
45
46
47
48
49
50
51
52
53
54
55
56
57
58
59
60
61
62
63
64
65
66
67
68
69
70
71
72
73
74
75
76
77
78
79
80
81
82
83
84
85
86
87
88
89
90
91
92
93
94
95
96
97
98
99
100
101
102
103
104
105
106
107
108
109
110
111
112
113
114
115
116
117
118
119
120
121
122
123
124
125
126
127
128
129
130
131
132
133
134
135
136
137
138
139
140
141
142
143
144
145
146
147
148
149
150
151
152
153
154
155
156
157
158
159
160
161
162
163
164
165
166
167
168
169
170
171
172
173
174
175
176
177
178
179
180
181
182
183
184
185
186
187
188
189
190
191
192
193
194
195
196
197
198
199
200
201
202
203
204
205
206
207
208
209
210
211
212
213
214
215
216
217
218
219
220
221
222
223
224
225
226
227
228
229
230
231
232
233
234
235
236
237
238
239
240
241
242
243
244
245
246
247
248
249
250
251
252
253
254
255
256
257
258
259
260
261
262
263
264
265
266
267
268
269
270
271
272
273
274
275
276
277
278
279
280
281
282
283
284
285
286
287
288
289
290
291
292
293
294
295
296
297
298
299
300
301
302
303
304
305
306
307
308
309
310
311
312
313
314
315
316
317
318
319
320
321
322
323
324
325
326
327
328
329
330
331
332
333
334
335
336
337
338
339
340
341
342
343
344
345
346
347
348
349
350
351
352
353
354
355
356
357
358
359
360
361
362
363
364
365
366
367
368
369
370
371
372
373
374
375
376
377
378
379
380
381
382
383
384
385
386
387
388
389
390
391
392
393
394
395
396
397
398
399
400
401
402
403
404
405
406
407
408
409
410
411
412
413
414
415
416
417
418
4

- 1 [36] Bhunia MK, Yamauchi K, Takanabe K. Harvesting solar light with crystalline
2
3 carbon nitrides for efficient photocatalytic hydrogen evolution. *Angew Chem Int*
4
5
6 Ed 2014;53:11001–5.
7
8
- 9 [37] Kang YY, Yang YQ, Yin LC, Kang XD, Wang LZ, Liu G, Cheng HM. Selective
10
11 breaking of hydrogen bonds of layered carbon nitride for visible light
12
13 photocatalysis. *Adv Mater* 2016;28: 6471–7.
14
15
16
- 17 [38] Ou HH, Lin LL, Zheng Y, Yang PJ, Fang YX, Wang XC. Tri-s-triazine-based
18
19 crystalline carbon nitride nanosheets for an improved hydrogen evolution. *Adv*
20
21
22 *Mater* 2017;29:1700008–13.
23
24
- 25 [39] Ren W, Cheng JJ, Ou HH, Huang CJ, Titirici MM, Wang XC. Enhancing
26
27 visible-light hydrogen evolution performance of crystalline carbon nitride by
28
29 defect engineering. *ChemSusChem* 2019;12:3257–62.
30
31
32
- 33 [40] Chen L, Zhu DY, Li JT, Wang XX, Zhu JF, Francis PS, Zheng YH. Sulfur and
34
35 potassium co-doped graphitic carbon nitride for highly enhanced photocatalytic
36
37 hydrogen evolution. *Appl Catal B Environ* 2020;273:119050–8.
38
39
40
- 41 [41] Li Y, Zhang DN, Feng XH, Xiang QJ. Enhanced photocatalytic hydrogen
42
43 production activity of highly crystalline carbon nitride synthesized by
44
45 hydrochloric acid treatment. *Chinese J Catal* 2020;41:21–30.
46
47
48
- 49 [42] Mase K, Yoneda M, Yamada Y, Fukuzumi S. Seawater usable for production and
50
51 consumption of hydrogen peroxide as a solar fuel. *Nat Commun* 2016;7:11470–6.
52
53
54
- 55 [43] Xiong T, Cen W, Zhang Y, Dong F. Bridging the g-C₃N₄ interlayers for enhanced
56
57 photocatalysis. *ACS Catal* 2016;6:24622472.
58
59
60
61
62
63
64
65

- 1 [44] Zhang GG, Lin LH, Li GS, Zhang YF, Savateev A, Zafeiratos S, Wang XC,
2
3 Antonietti M. Ionothermal synthesis of triazine-heptazine-based copolymers with
4
5
6 apparent quantum yields of 60% at 420 nm for solar hydrogen production from
7
8
9 “sea water”. *Angew Chem Int Ed* 2018;57:9372–6.
- 10
11 [45] Jing HJ, You MZ, Yi SS, Li T, Ji HP, Wang Y, Zhang ZT, Zhang R, Chen DL,
12
13
14 Yang HM. Precursor-engineering coupled microwave-molten-salt strategy highly
15
16
17 enhances photocatalytic hydrogen evolution performance of g-C₃N₄
18
19
20 nanostructures. *ChemSusChem* 2020;13:827–37.
- 21
22 [46] Gao ZQ, Chen KY, Wang L, Bai B, Liu H, Wang QZ. Aminated flower-like
23
24
25 ZnIn₂S₄ coupled with benzoic acid modified g-C₃N₄ nanosheets via covalent
26
27
28 bonds for ameliorated photocatalytic hydrogen generation. *Appl Catal B Environ*
29
30
31 2020;268:118462–70.
- 32
33 [47] Fan XQ, Zhang LX, Wang M, Huang WM, Zhou YJ, Li ML, Cheng RL, Shi JL.
34
35
36 Constructing carbon-nitride-based copolymers via Schiff base chemistry for
37
38
39 visible-light photocatalytic hydrogen evolution. *Appl Catal B Environ*
40
41
42 2016;182:68–73.
- 43
44 [48] Martin DJ, Qiu KP, Shevlin SA, Handoko AD, Chen XW, Guo ZX, Tang JW.
45
46
47 Highly efficient photocatalytic H₂ evolution from water using visible light and
48
49
50 structure-controlled graphitic carbon nitride. *Angew Chem Int Ed* 2014;126:9394–
51
52
53 9.
- 54
55 [49] Chen YL, Qu Y, Zhou X, Li DZ, Xu P, Sun JM. Phenyl-bridged graphitic carbon
56
57
58 nitride with a porous and hollow sphere structure to enhance dissociation of
59
60
61
62
63
64
65

1 photogenerated charge carriers and visible-light-driven H₂ generation. ACS Appl
2 Mater Interfaces 2020;12:41527–37.
3
4

5
6 [50] Yang J, Liang YJ, Li K, Yang G, Wang K, Xu R, Xie XJ. One-step synthesis of
7 novel K⁺ and cyano groups decorated triazine-/heptazine-based g-C₃N₄ tubular
8 homojunctions for boosting photocatalytic H₂ evolution. Appl Catal B Environ
9 2020;262:118252–63.
10
11

12
13 [51] Feng CY, Tang L, Deng YC, Wang JJ, Luo J, Liu YN, Ouyang XL, Yang HR,
14 Yu JF, Wang JJ. Synthesis of leaf-vein-like g-C₃N₄ with tunable band structures
15 and charge transfer properties for selective photocatalytic H₂O₂ evolution. Adv
16 Funct Mater 2020;30:2001922–34.
17
18

19
20 [52] Güy N, Çakar S, Özacar M. Comparison of palladium/zinc oxide photocatalysts
21 prepared by different palladium doping methods for congo red degradation. J
22 Colloid Interface Sci 2016;466:128–37.
23
24

25
26 [53] Andrew Lin KY, Lin JT. Ferrocene-functionalized graphitic carbon nitride as an
27 enhanced heterogeneous catalyst of Fenton reaction for degradation of Rhodamine
28 B under visible light irradiation. Chemosphere 2017;182:54–64.
29
30
31
32
33
34
35
36
37
38
39
40
41
42
43
44
45
46
47
48
49
50
51
52
53
54
55
56
57
58
59
60
61
62
63
64
65

1 **Figure captions**

2
3 **Fig. 1.** (a) XRD patterns, (b) ^{13}C CP-MAS NMR of KCN and KBCN samples, (c)
4
5 FTIR spectra of prepared PCN, BCN, KCN, and KBCN samples.
6

7
8
9 **Fig. 2.** High-resolution XPS spectra of (a) C1s, (b) N1s, (c) O1s, and (d) K2p in PCN
10
11 and KBCN samples.
12

13
14 **Fig. 3.** (a) SEM, (b) TEM, (c) HRTEM, and HAADF-STEM images of KBCN, as
15
16 well as the elemental mapping of C, N, O, and K.
17

18
19
20 **Fig. 4.** (a) UV-vis DRS, (b) Photocatalytic production of H_2O_2 in pure water, (c)
21
22 Photocatalytic decomposition of H_2O_2 , (d) Reusability of KBCN sample in H_2O_2
23
24 production.
25

26
27
28 **Fig. 5.** Results of degradation efficiencies and stability tests for RhB (a, b) and CR (c,
29
30 d) over KBCN.
31

32
33
34 **Fig. 6.** Theoretical calculated LUMO (a, c) and HOMO (b, d) for KCN and KBCN,
35
36 respectively. Gray, blue, red, purple, and white spheres represent the C, N, O, K, and
37
38 H atoms, respectively.
39

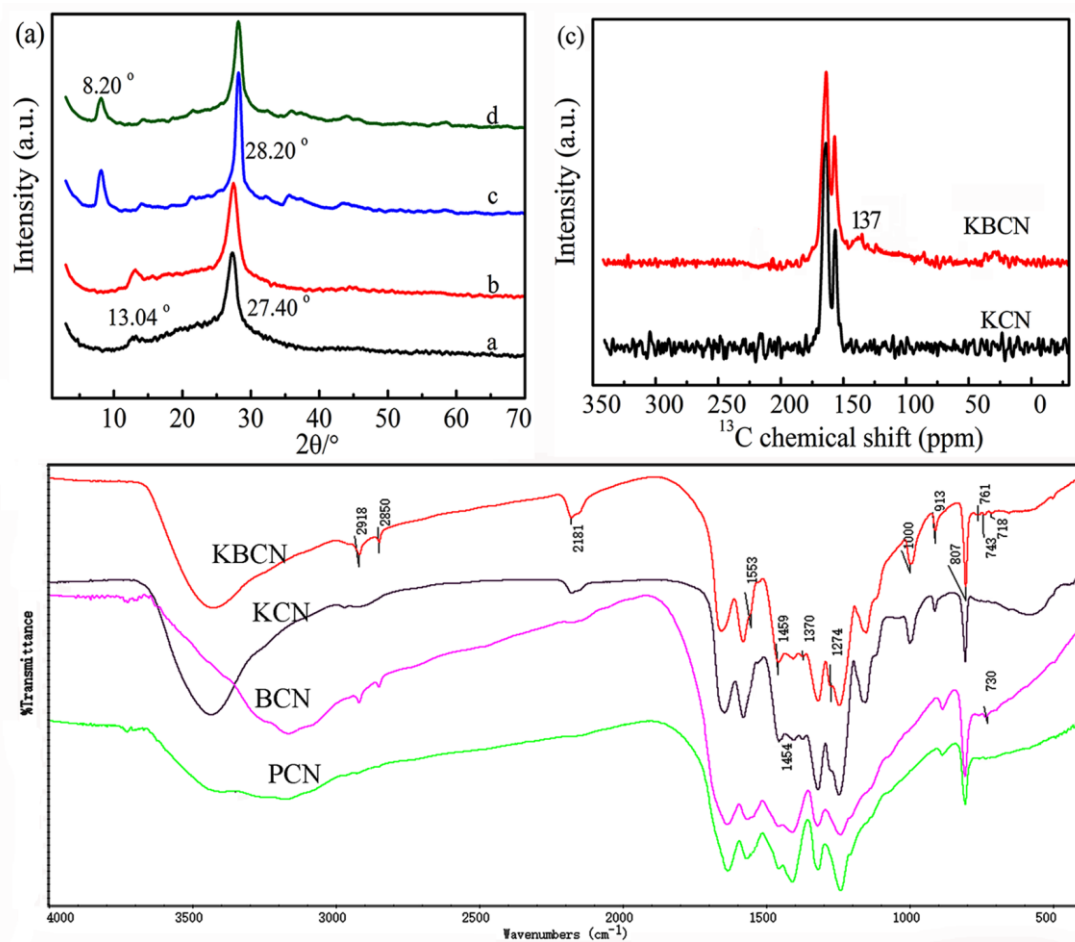
40
41
42 **Fig. 7.** Degradation efficiencies of (a) RhB and (b) CR in various conditions, (c) ESR
43
44 spectra of DMPO- $\cdot\text{OH}$ adducts and (d) Fluorescence spectra of TA in the presence of
45
46 KBCN.
47

48
49
50 **Fig. 8.** Schematic of Fenton-like degradation of RhB and CR with in situ-generated
51
52 H_2O_2 for KBCN.
53

54
55
56 **Fig. 9.** Degradation pathway of CR over KBCN.
57

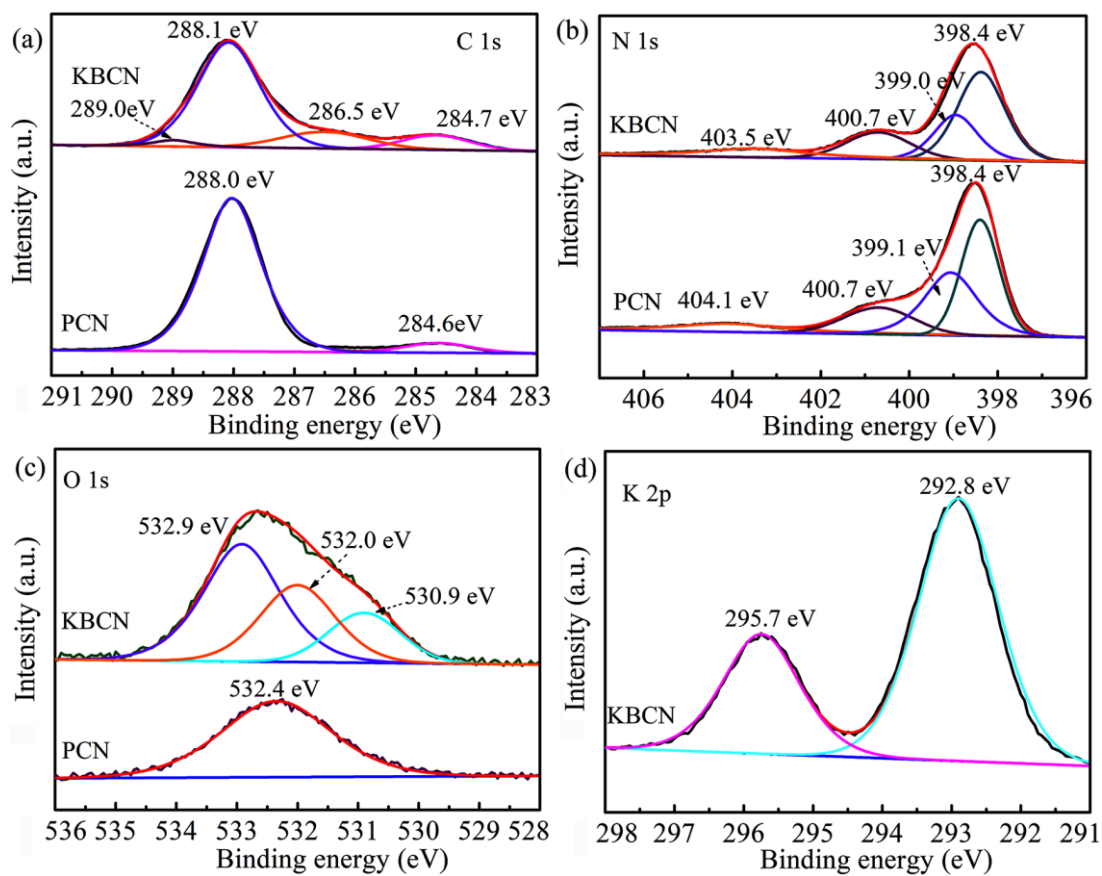
58
59 **Fig. 10.** Degradation pathway of RhB over KBCN.
60
61
62
63
64
65

Figure 1



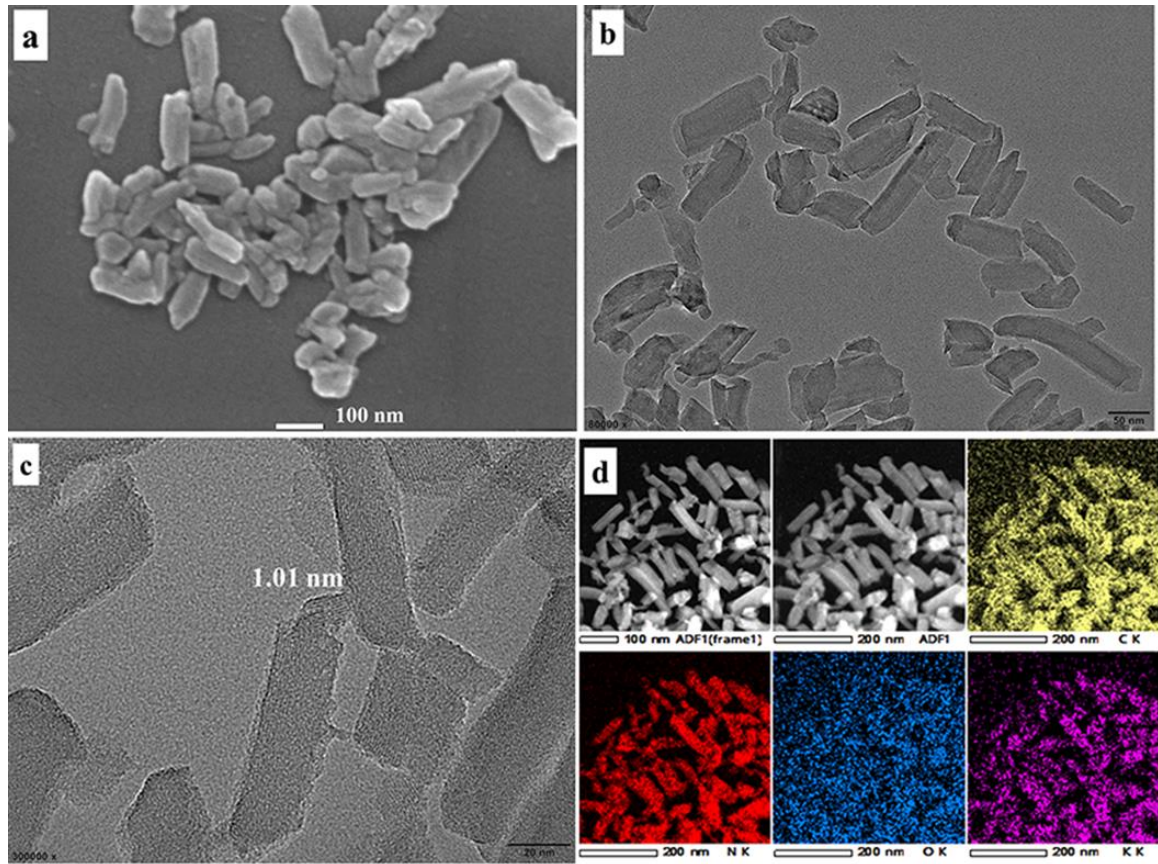
1
2
3
4
5
6
7
8
9
10
11
12
13
14
15
16
17
18
19
20
21
22
23
24
25
26
27
28
29
30
31
32
33
34
35
36
37
38
39
40
41
42
43
44
45
46
47
48
49
50
51
52
53
54
55
56
57
58
59
60
61
62
63
64
65

Figure 2

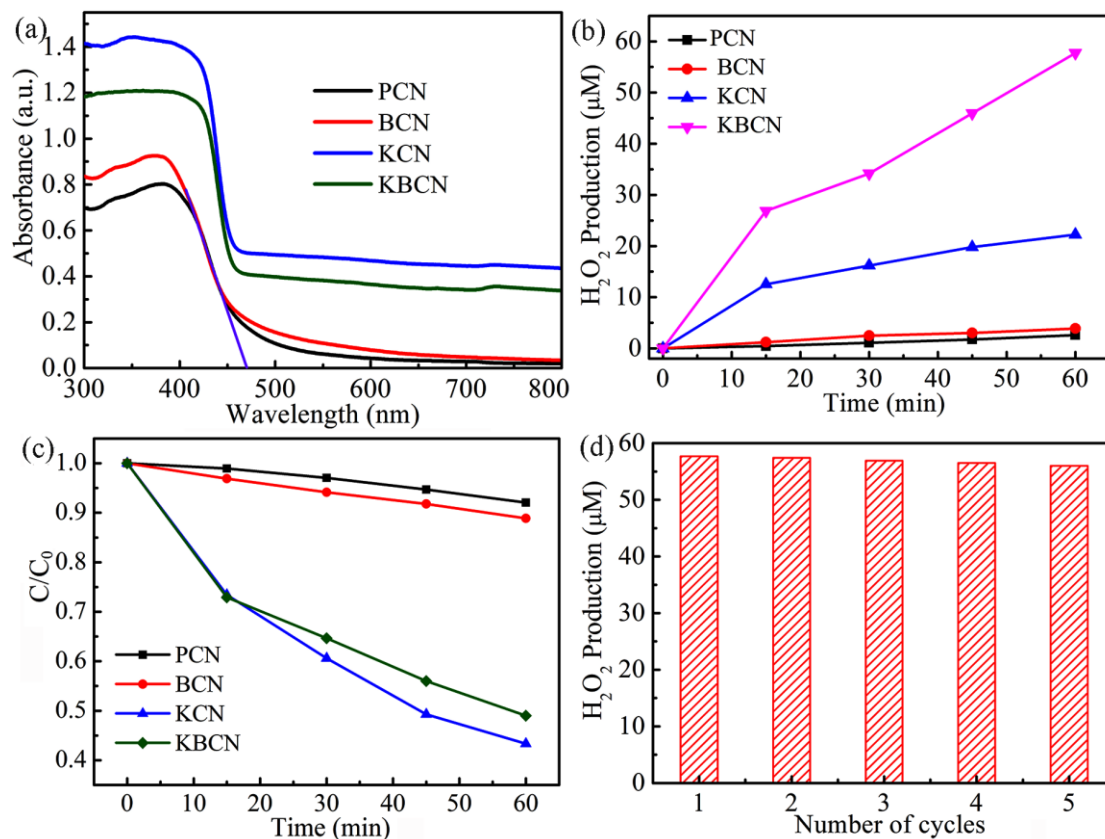


1
2
3
4
5
6
7
8
9
10
11
12
13
14
15
16
17
18
19
20
21
22
23
24
25
26
27
28
29
30
31
32
33
34
35
36
37
38
39
40
41
42
43
44
45
46
47
48
49
50
51
52
53
54
55
56
57
58
59
60
61
62
63
64
65

1
2
3
4 **Figure 3**
5



1
2
3
4 **Figure 4**
5



1
2
3
4
5
Figure 5

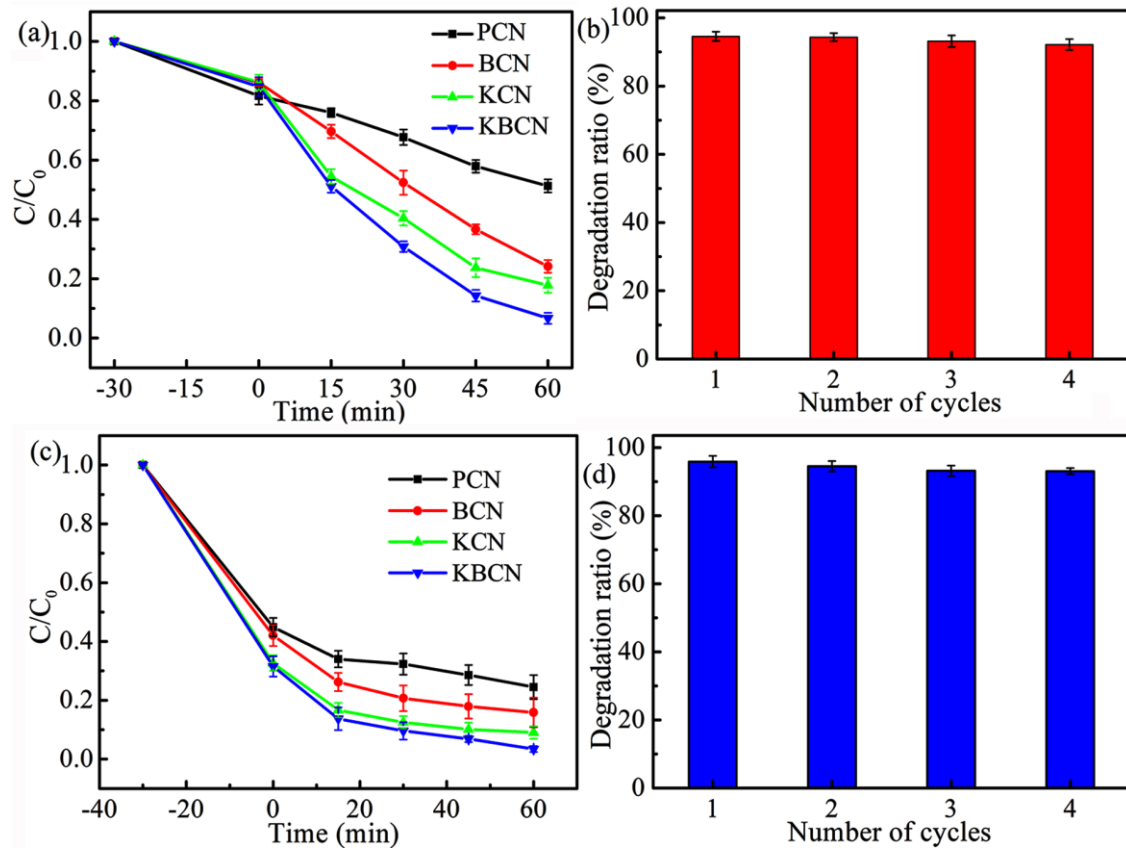


Figure 6

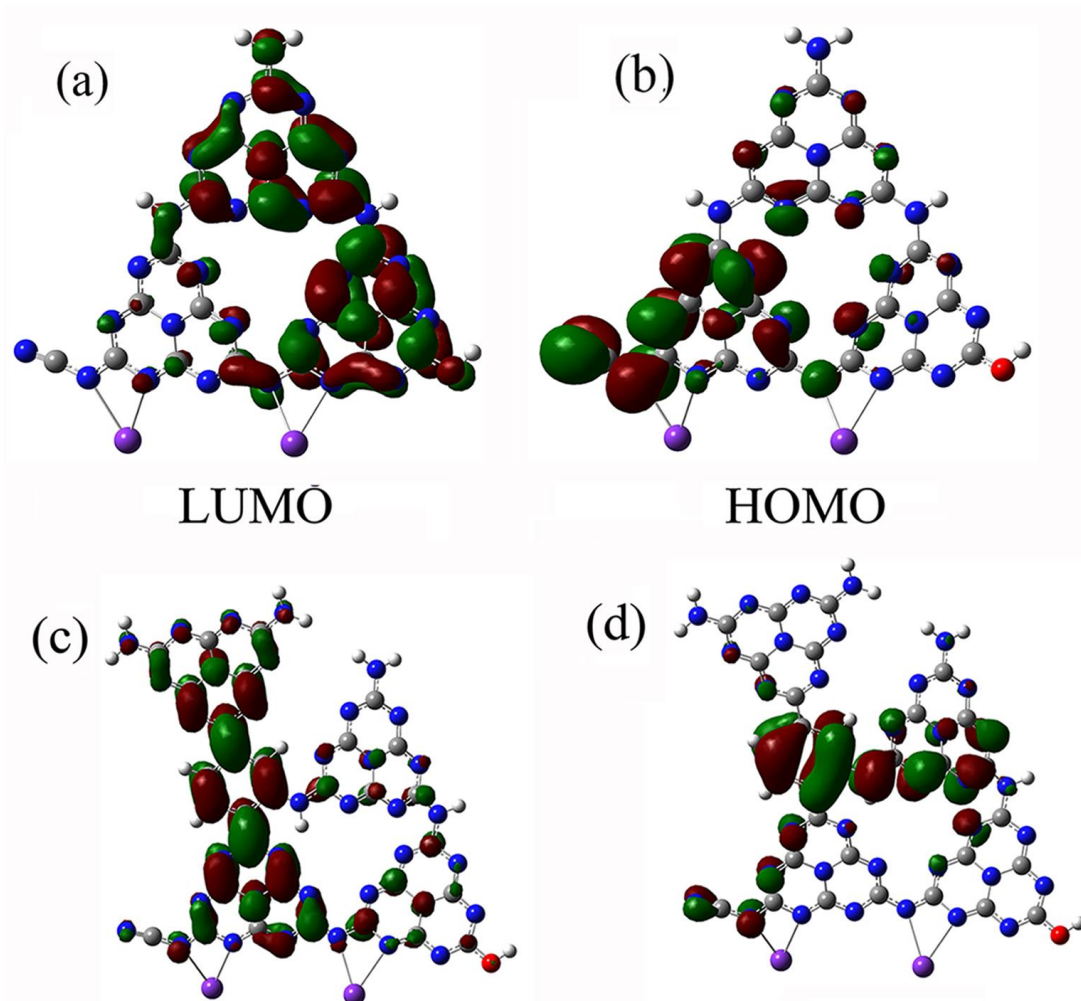


Figure 7

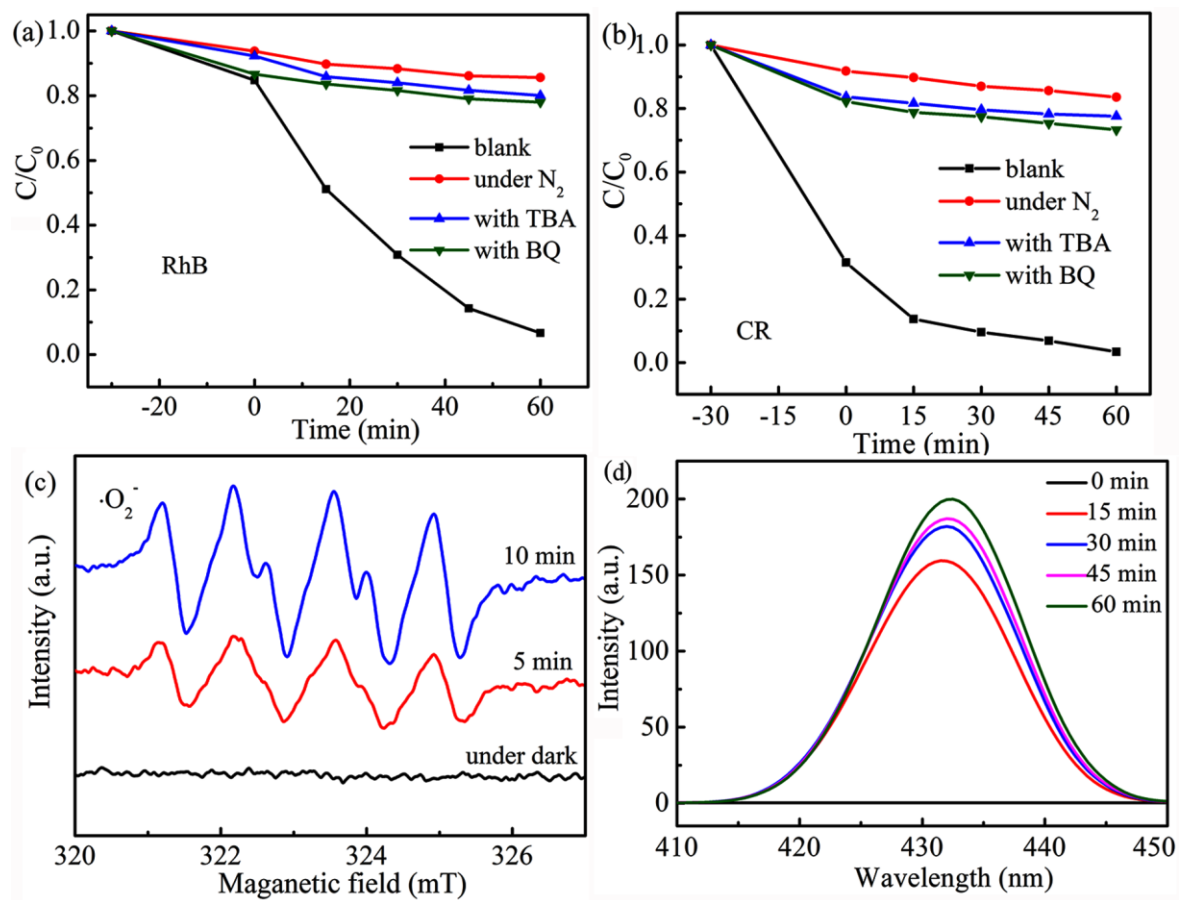
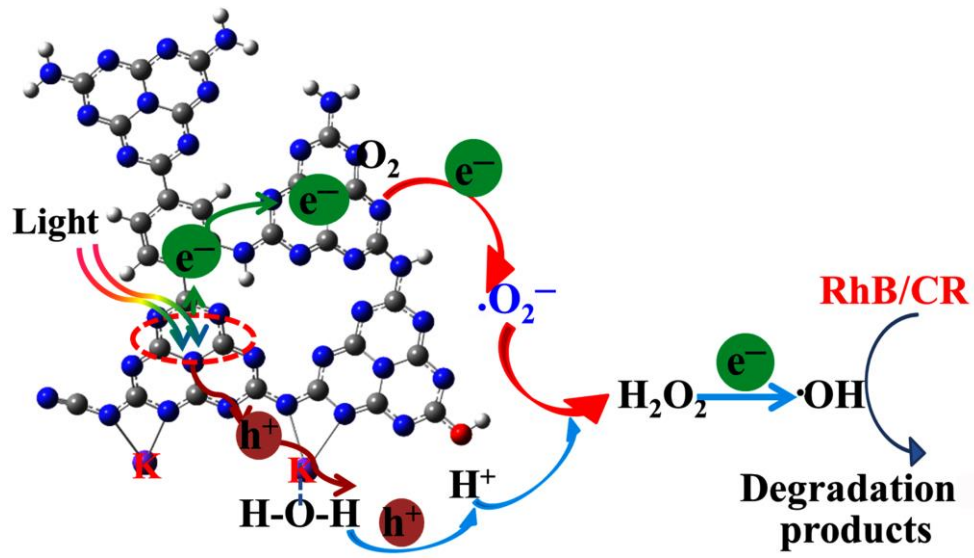


Figure 8



1
2
3
4
5
6
7
8
9
10
11
12
13
14
15
16
17
18
19
20
21
22
23
24
25
26
27
28
29
30
31
32
33
34
35
36
37
38
39
40
41
42
43
44
45
46
47
48
49
50
51
52
53
54
55
56
57
58
59
60
61
62
63
64
65

1
2
3
4
5
6
7
8
9
10
11
12
13
14
15
16
17
18
19
20
21
22
23
24
25
26
27
28
29
30
31
32
33
34
35
36
37
38
39
40
41
42
43
44
45
46
47
48
49
50
51
52
53
54
55
56
57
58
59
60
61
62
63
64
65

Figure 9

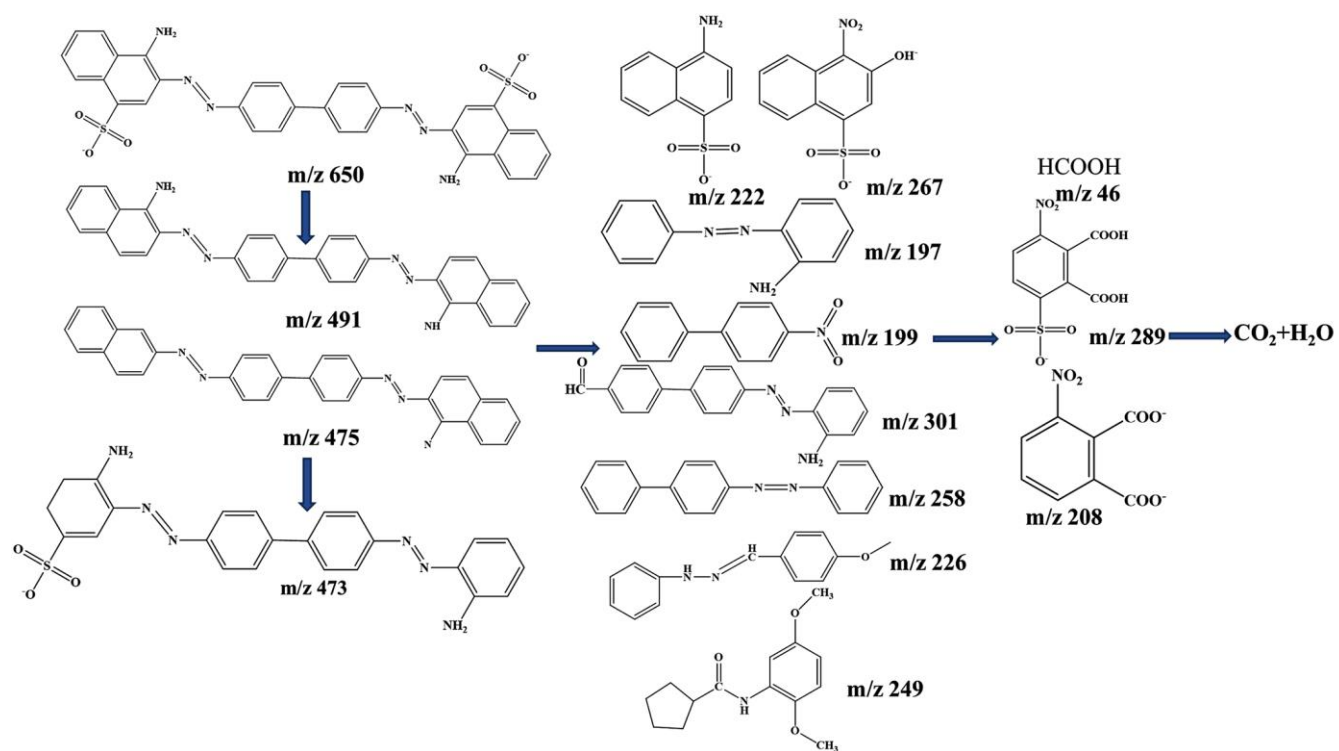
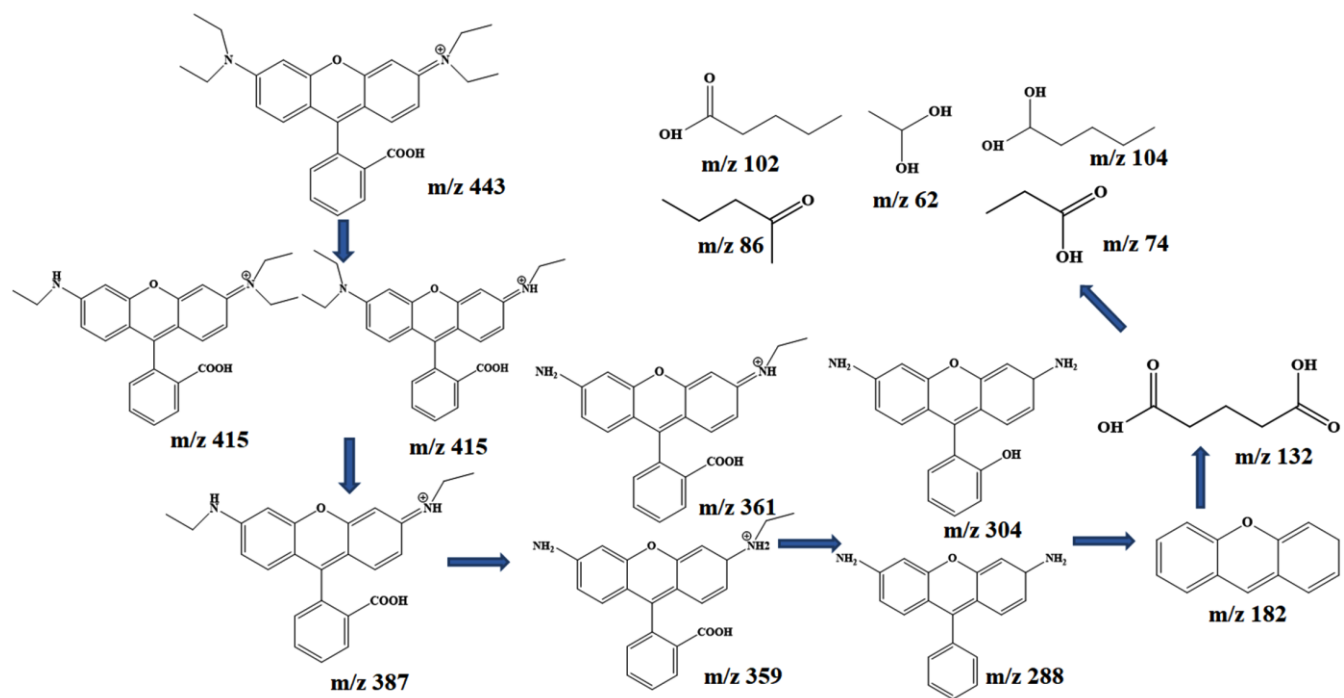


Figure 10





Click here to access/download
Supplementary Material
Supplementary Materials.docx



Graphical abstract

